Journal of Nonlinear Science (2020) 30:2405–2427
https://doi.org/10.1007/s00332-018-9489-3

Journal of Nonlinear Science

The Kuramoto Model on Power Law Graphs: Synchronization and Contrast States

Georgi S. Medvedev[1] · **Xuezhi Tang**[2]

Received: 31 March 2018 / Accepted: 16 August 2018 / Published online: 8 September 2018

Abstract

The relation between the structural properties of the network and its dynamics is a central question in the analysis of dynamical networks. It is especially relevant for complex networks found in real-world applications. This work presents mathematically rigorous analysis of coupled dynamical systems on power law graphs. Specifically, we study large systems of coupled Kuramoto phase oscillators. In the limit as the size of the network tends to infinity, we derive analytically tractable mean field partial differential equation for the probability density function describing the state of the coupled system. The mean field limit is used to establish an explicit formula for the synchronization threshold for coupled phase oscillators with randomly distributed intrinsic frequencies. Furthermore, we study stable spatial patterns generated by the Kuramoto model with repulsive coupling. In particular, we identify a family of stable steady-state solutions having multiple regions with distinct statistical properties. We call these solutions contrast states. Like chimera states, contrast states exhibit coexisting regions of highly localized (coherent) behavior and highly irregular (incoherent) distribution of phases. We provide a detailed mathematical analysis of contrast states in the KM using the Ott–Antonsen ansatz. The analysis of synchronization and contrast states provides new insights into the role of power law connectivity in shaping dynamics of coupled dynamical systems. In particular, we show that despite sparse connectivity, power law networks possess remarkable synchronizability: the synchronization threshold can be made arbitrarily low by varying the parameter of the power law distribution.

Keywords Coupled oscillators · Synchronization · Chimera state · Scale free graph · Graph limit · Mean field limit

Communicated by Paul Newton.

✉ Georgi S. Medvedev
medvedev@drexel.edu

Extended author information available on the last page of the article

1 Introduction

Coupled dynamical systems on graphs serve as mathematical models of various technological physical, biological, social, and economic networks (Porter and Gleeson 2016). Examples include neuronal and genetic networks and models of flocking in life sciences (Motsch and Tadmor 2014); power and information networks and consensus protocols in technology (Medvedev 2012); and economic and social networks and models of opinion dynamics in social sciences (Porter and Gleeson 2016). This list can be continued. Numerical simulations and mathematical analysis of coupled systems provided many important insights into the mechanisms underlying collective dynamics in complex networks. In the last two decades, there have been a remarkable progress in understanding classical phenomena such as synchronization and phase locking in complex networks (Chiba and Nishikawa 2011; Strogatz 2000; Wiley et al. 2006; Medvedev and Tang 2015; Medvedev and Douglas Wright 2017), and the discoveries of new effects in the dynamics of networks such as chimera states (Kuramoto and Battogtokh 2002; Abrams and Strogatz 2006; Omelchenko 2013). The research on dynamical networks has been fueled by the desire for better understanding the link between the structure of a network and its dynamics. This is the main motivation of our work.

Real-world networks feature a rich variety of connectivity patterns. Scale-free networks have been singled out in the network science community for their nontrivial structure and compelling applications. The latter include the world wide web and scientific citation network among other physical, biological, and social networks (Barabási and Albert 1999). Scale-free graphs are characterized by power law asymptotics of the degree distribution. For this reason, they are also called power law graphs. In practice, power law distribution is determined by statistical methods. Different combinatorial algorithms such as the preferential attachment (see, e.g., Borgs et al. 2011) and Chung and Lu (2002) methods are used to generate computational models of scale-free graphs. Dynamical systems on the graphs generated by these methods are difficult to study analytically. Consequently, there are few mathematical results on the dynamics of coupled systems on scale-free graphs. The goal of this paper is to rectify this situation. We introduce a new framework for modeling and analyzing coupled systems on scale-free graphs. For concreteness, we study coupled Kuramoto phase oscillators. The same approach applies to other models of interacting dynamical systems on graphs. For the KM on power law graphs, we derive an analytically tractable mean field limit, which describes dynamics of the coupled system in the limit as the number of oscillators tends to infinity. The mean field limit is used to study two problems: synchronization in the KM with random intrinsic frequencies (Strogatz 2000) and attractors in repulsively coupled KM with identical intrinsic frequencies. For each problem, we identify the role of power law connectivity in shaping the corresponding dynamical regime.

The KM of coupled phase oscillators is one of the most successful mathematical models for studying collective dynamics and synchronization (Kuramoto 1975). It captures the essential features of dynamics of weakly coupled limit cycle oscillators (Hoppensteadt and Izhikevich 1997) and has many interesting applications in physical and biological sciences (Strogatz 2000). In the synchronization problem, the intrinsic

frequencies of the individual oscillators are assumed to be taken from a probability distribution with density function g. Then, one wants to find a critical value of the coupling strength, which marks the transition from to synchronization. For the classical KM on complete graphs, Kuramoto found the critical value $K_c = 2\pi/g(0)$. Kuramoto's self-consistent analysis recently received a rigorous mathematical justification in Chiba and Nishikawa (2011), Chiba (2015). In the present paper, we use the results in Chiba and Medvedev (2016), which extend the techniques from Chiba and Nishikawa (2011) to the analysis of the KM on graphs. Using these techniques, we obtain an explicit formula for the onset of synchronization for scale-free graphs. Interestingly, we find that the KM on sparse power law graphs can have lower synchronization threshold than on dense graphs. In fact, the synchronization threshold can be made arbitrarily low by controlling the parameter of the power law distribution.

The second problem considered in this paper deals with attractors in repulsively coupled KM with identical frequencies on power law graphs. We find that this system has a variety of stable steady-state solutions forming striking spatial patterns with well-defined statistical properties. We demonstrate existence of a class of such solutions having well-defined regions of coherent and incoherent distribution of phases, like in chimera states. We show that the phases in these regions are distributed according to distinct probability laws. We call such solutions contrast states, because they combine statistically distinct modes of behavior. Further, we show that in the continuum limit contrast states form a continuous family. In numerical simulations, different contrast states can be obtained as asymptotic states of the KM by varying (on a continuous scale) the distribution of random initial conditions. To study these solutions analytically, we employ the mean field limit for the KM on graphs (Chiba and Medvedev 2016; Kaliuzhnyi-Verbovetskyi and Medvedev 2018) and the Ott–Antonsen ansatz (Ott and Antonsen 2008).

The organization of the paper is as follows. In the next section, we explain the W-random graph model (Lovász and Szegedy 2006; Borgs et al. 2014). This is the key ingredient in our model of coupled dynamical systems on power law graphs. The W-random graph model affords a convenient analytically tractable continuum limit. In the next section, after explaining W-random graphs, we formulate the KM on the power law graphs following (Kaliuzhnyi-Verbovetskyi and Medvedev 2017) and review the mathematical background of the mean field equation for the KM on graphs following (Chiba and Medvedev 2016) (see also Kaliuzhnyi-Verbovetskyi and Medvedev 2018). Section 3 deals with the synchronization problem for the KM on power law graphs, and Sect. 4—with attractors in the repulsively coupled model. We conclude with brief discussion in Sect. 5.

2 The Model and Its Approximations

W-random graphs provide a convenient framework for deriving the continuum limit of the KM on convergent families of graphs (Medvedev 2014a, b; Kaliuzhnyi-Verbovetskyi and Medvedev 2017; Chiba and Medvedev 2016). In this section, we explain the W-random graph model adapted from Borgs et al. (2014), which will be used below.

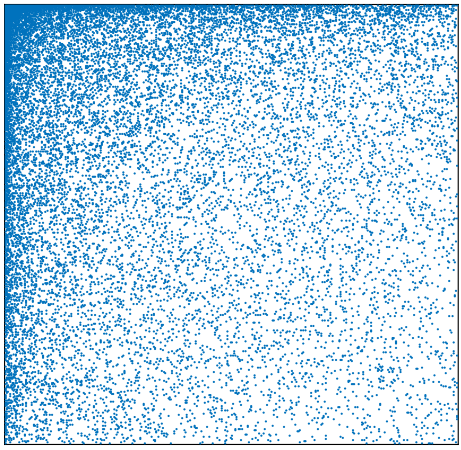

Fig. 1 The pixel plot of the adjacency matrix of a power law graph. Each pixel represents a nonzero entry of the adjacency matrix

Let $W(x, y) = (xy)^{-\alpha},\ \rho_n = n^{-\beta},\ 0 < \alpha < \beta < 1/2$, and

$$X_n = \{x_{n0}, x_{n1}, x_{n2}, \ldots, x_{nn}\},\ x_{ni} = i/n,\ i = 0, 1, \ldots, n. \tag{2.1}$$

and

$\Gamma_n = G(W, \rho_n, X_n)$ stands for a random graph with the node set $V(\Gamma_n) = [n] := \{1, 2, \ldots, n\}$ and the edge set $E(\Gamma_n)$ defined as follows. The probability that $\{i, j\}$ forms an edge is

$$\mathbb{P}\left(\{i, j\} \in E(\Gamma_n)\right) = \rho_n \bar{W}_n(x_{ni}, x_{nj}) =: \rho_n \bar{W}_{nij},\ i, j \in [n], \tag{2.2}$$

where[1]

$$\bar{W}_n(x, y) = \rho_n^{-1} \wedge W(x, y). \tag{2.3}$$

The decision whether a given pair of nodes is included in the edge set is made independently from other pairs. In other words, $G(W, \rho_n, X_n)$ is a product probability space

$$(\Omega_n = \{0, 1\}^{n(n+1)/2}, 2^{\Omega_n}, \mathbb{P}). \tag{2.4}$$

By $\Gamma_n(\omega)$, $\omega \in \Omega_n$, we will denote a random graph drawn from the probability distribution $G(W, \rho_n, X_n)$ (Fig. 1).

Lemma 2.1 (Kaliuzhnyi-Verbovetskyi and Medvedev 2017) *$\Gamma_n = G(W, \rho_n, X_n)$ has the following properties:*

(A) *The expected degree of node $i \in [n]$ of Γ_n is*[2]

$$\mathbb{E}_\omega \deg_{\Gamma_n}(i) = (1 - \alpha)^{-1} n^{1+\alpha-\beta} i^{-\alpha}(1 + o(1)). \tag{2.5}$$

[1] Throughout this paper, we use $a \wedge b$ and $a \vee b$ to denote $\min\{a, b\}$ and $\max\{a, b\}$, respectively.

[2] Here and below, $\mathbb{E}_\omega$ denotes the mathematical expectation with respect to the probability space (2.4) underlying the random graph model.

(B) *The expected edge density of* Γ_n *is* $(1-\alpha)^{-2}n^{-\beta}(1+o(1))$.

Let $\Gamma_n = \Gamma_n(\omega), \omega \in \Omega_n$, be a random graph model taken from the probability distribution $G(W, \rho_n, X_n)$. The KM on Γ_n is defined as follows:[3]

$$\dot{u}_{ni} = \eta_i + \frac{K}{n\rho_n}\sum_{j=1}^{n}\xi_{nij}(\omega)\sin(u_{nj}-u_{ni}), \quad i \in [n], \tag{2.6}$$

where $u_{ni}, i \in [n]$, stands for the phase of oscillator i and η_i is its intrinsic frequency. Until Sect. 4, we assume that the intrinsic frequencies are drawn form a continuous probability distribution with density g. $\xi_{nij}(\omega) = \mathbf{1}_{E(\Gamma_n(\omega))}(\{i,j\})$ is a Bernoulli random variable, which takes value 1 when $\{i,j\}$ is an edge of Γ_n. K controls the strength of coupling. For sparse graphs like the power law graph $\Gamma_n = G(W, \rho_n, X_n)$, the edge density vanishes as $n \to \infty$ (cf. Lemma 2.1). Thus, one needs to rescale the coupling term appropriately so that it does not vanish as $n \to \infty$. The scaling factor ρ_n is used to make the continuum limit of (2.6) nondegenerate.

The analysis of (2.6) relies on several approximations, which we discuss next. Note that the right-hand side of (2.6) depends on the realization of the random graph model $\Gamma_n = G(W, \rho_n, X_n)$. Thus, (2.6) is a system of ordinary differential equations with random coefficients. As a first step in analyzing (2.6), we substitute (2.6) by the averaged model, which approximates the random KM (2.6). Specifically, we average the right-hand side of (2.6) over all possible realizations of Γ_n:

$$\dot{\bar{v}}_{ni}(t) = F_{ni}(\bar{v}_n), \;\; v_n(t) = (\bar{v}_{n1}(t), \bar{v}_{n2}(t), \ldots, \bar{v}_{nn}(t)), \quad i \in [n], \tag{2.7}$$

where

$$\begin{aligned} F_{ni}(v) &= \mathbb{E}_{\,\omega}\left\{\eta_i + K(n\rho_n)^{-1}\sum_{j=1}^{n}\xi_{nij}(\omega)\sin(v_{nj}-v_{ni})\right\} \\ &= \eta_i + K(n\rho_n)^{-1}\sum_{j=1}^{n}\mathbb{E}_{\,\omega}\left(\xi_{nij}(\omega)\right)\sin(v_{nj}-v_{ni}) \\ &= \eta_i + Kn^{-1}\sum_{j=1}^{n}\bar{W}_{nij}\sin(v_{nj}-v_{ni}), \end{aligned}$$

where we used (2.2). Recall that $\mathbb{E}_{\,\omega}$ stands for the mathematical expectation with respect to the probability space (2.4).

Thus, the averaged model has the following form

$$\dot{\bar{v}}_{ni} = \eta_i + Kn^{-1}\sum_{j=1}^{n}\bar{W}_{nij}\sin(\bar{v}_{nj}-\bar{v}_{ni}), \quad i \in [n]. \tag{2.8}$$

[3] Equation (2.6) is derived from a system of weakly coupled oscillators (Kuramoto 1975; Hoppensteadt and Izhikevich 1997).

We approximate (2.8) by

$$\dot{v}_{ni} = \eta_i + Kn^{-1} \sum_{j=1}^{n} W_{nij} \sin(v_{nj} - v_{ni}), \quad i \in [n], \tag{2.9}$$

where

$$W_{nij} = W(x_{ni}, x_{nj}) = (x_{ni} x_{nj})^{-\alpha}, \quad (i, j) \in [n]^2. \tag{2.10}$$

The next step is the derivation of the mean field approximation for (2.9), which captures its dynamics in the limit as $n \to \infty$:

$$\frac{\partial}{\partial t} \rho(t, u, \eta, x) + \frac{\partial}{\partial u} \{\rho(t, u, \eta, x) V(t, u, \eta, x)\} = 0 \tag{2.11}$$

where

$$V(t, u, \eta, x) = \eta + K \int_I \int_{\mathbb{R}} \int_{\mathbb{S}} W(x, y) \sin(v - u) \rho(t, v, \eta, y) \mathrm{d}v \mathrm{d}\eta \mathrm{d}y \tag{2.12}$$

Here, $\rho(t, u, \eta, x)$ stands for a probability density function on $G = \mathbb{S} \times \mathbb{R} \times I$ parametrized by time $t \in \mathbb{R}^+$. It aims to describe the distribution of the oscillators of the discrete model (2.6) at time t, provided both initial value problems (IVPs) for (2.6) and (2.11) are initialized appropriately.

The mean field limit has been very useful in studies of interacting dynamical systems (Golse 2016; Strogatz and Mirollo 1991). It has been instrumental in the analysis of synchronization and chimera states in the KM (Strogatz 2000; Omelchenko 2013) among many other dynamical regimes. For the original KM on complete graphs, the rigorous mathematical justification of the mean field equation (2.11) was given by Lancellotti (2005). It relies on the classical theory for the Valsov equation (Neunzert 1978). For the KM on graphs, the justification of the mean field limit was developed in Chiba and Medvedev (2016), Kaliuzhnyi-Verbovetskyi and Medvedev (2018). Although the results in these papers do not apply to the KM with singular kernel $W(x, y) = (xy)^{-\alpha}$, $0 < \alpha < 1/2$, the proof of the mean field limit in Kaliuzhnyi-Verbovetskyi and Medvedev (2018) can be extended to cover the case $W \in L^2(I^2)$. This is work in progress. Likewise, at the moment we are unable to provide a rigorous justification of averaging for the model at hand. However, results for closely related models are available in Kaliuzhnyi-Verbovetskyi and Medvedev (2018, Appendix A) (see also Medvedev 2018, Theorem 3.1). In fact, Theorem 3.1 of Medvedev (2018) justifies averaging for a modification of (2.6) considered in § 4.7.

If W is replaced by the truncated kernel $W_C(x, y) = C \wedge (xy)^{-\alpha}$ for arbitrary $C > 0$ then the interpretation of the mean field limit in Chiba and Medvedev (2016) carries over to the problem at hand. Using the truncated kernel does not limit the applications of our results very much, as many effects considered in this work can be achieved with W_C instead of W. For the sake of completeness, the remainder of this section we explain the mathematical meaning of the mean field equation (2.11) and its relation to the discrete system (2.9) assuming that $W := W_C$ for sufficiently large $C > 0$.

Consider the following initial condition for (2.11)

$$\rho(0, u, \eta, x) = \rho^0(u, \eta, x)g(\eta), \tag{2.13}$$

where the nonnegative $\rho^0 \in L^1(G)$ satisfies

$$\int_{\mathbb{S}} \rho^0(u, \eta, x)\mathrm{d}u = 1 \quad \forall(\eta, x) \in \mathbb{R} \times I. \tag{2.14}$$

Then, as shown in Chiba and Medvedev (2016), there is a unique weak solution of the IVP (2.11), (2.13). Moreover, $\rho(t, \cdot)$ is a probability density function on G for every $t \in [0, T]$. Thus, one can define the probability measure

$$\mu_t(A) = \int_A \rho(t, u, \eta, x)\mathrm{d}u\mathrm{d}\eta\mathrm{d}x, \quad A \in \mathcal{B}(G), \tag{2.15}$$

where $\mathcal{B}(G)$ stands for the collection of Borel subsets of G.

On the other hand, the solution of the IVP for discrete problem (2.9) defines the empirical measure

$$\mu_t^n(A) = n^{-1} \sum_{i=1}^{n} \mathbf{1}_A\left(\theta_{ni}(t), \eta_i, x_{ni}\right), \quad A \in \mathcal{B}(G). \tag{2.16}$$

The analysis in Chiba and Medvedev (2016), based on the Neunzert's theory for Vlasov equation (cf. Neunzert 1978), shows that

$$\sup_{t\in[0,T]} d_{\mathrm{BL}}(\mu_t^n, \mu_t) \to 0 \quad \text{as} \quad n \to \infty, \tag{2.17}$$

provided

$$d_{\mathrm{BL}}(\mu_0^n, \mu_0) \to 0 \quad \text{as} \quad n \to \infty, \tag{2.18}$$

Here, $d_{\mathrm{BL}}(\cdot, \cdot)$ stands for the bounded Lipschitz distance, which metrizes weak convergence for the space of Borel probability measures on G (Dudley 2002). Thus, if the initial distribution of oscillators (i.e., the initial conditions for (2.9)) converges weakly to μ_0 as $n \to \infty$, then the solution of the continuous problem (2.11), (2.13) approximates the distribution of oscillators around $\mathbb{S}$ for every $t \in [0, T]$. The same applies to the empirical measures generated by the discrete model on random graph (2.6) provided the averaging is justified (cf. Chiba and Medvedev 2016).

3 Synchronization

With the mean field limit (2.11) in hand, we are equipped to study dynamics of the KM on power law graphs (2.6). First, note that $\rho(t, u, \eta, x) = (2\pi)^{-1}g(\eta)$ is a steady-state solution of (2.11), corresponding to the state of the network with all oscillators

distributed uniformly around $\mathbb{S}$. We refer to this dynamical regime as the incoherent state.

Recall that $\alpha \in (0, 1/2)$ and assume that the probability density function $g(\eta)$ characterizing the distribution of intrinsic frequency η is even. Consider a self-adjoint operator $\mathcal{W} : L^2(I) \to L^2(I)$ defined by

$$\mathcal{W}[f] = \int_I W(\cdot, y) f(y) \mathrm{d}y, \quad f \in L^2(I). \tag{3.1}$$

Let $\mu_{\min}$ ($\mu_{\max}$) denote the smallest negative (largest positive) eigenvalue of $\mathcal{W}$. If all eigenvalues of $\mathcal{W}$ are positive (negative) set $\mu_{\min} := 0$ ($\mu_{\max} = 0$). Define

$$K_c^+ = \frac{2}{\pi g(0) \mu_{\max}(\mathcal{W})} \quad \text{and} \quad K_c^- = \frac{2}{\pi g(0) \mu_{\min}(\mathcal{W})}.$$

Theorem 3.1 (Chiba and Medvedev 2016) *The incoherent state is linearly stable for $K \in [K_c^-, K_c^+]$ and is unstable otherwise.*

To apply Theorem 3.1 to the problem at hand, we compute the eigenvalues of $\mathcal{W}$.

Lemma 3.2 *For $\alpha \in (0, 1/2)$, the spectrum of $\mathcal{W}$ consists of a simple eigenvalue $(1 - 2\alpha)^{-1}$ and the zero eigenvalue of infinite multiplicity.*

Proof Suppose ζ is an eigenvalue of $\mathcal{W}$, and $f \in L^2(I)$ is a corresponding eigenfunction. Then,

$$x^{-\alpha} \int_I y^{-\alpha} f(y) \mathrm{d}y = \zeta f(x).$$

If f is orthogonal to the subspace of $L^2(I)$ spanned by $x^{-\alpha}$, then $\zeta = 0$. Otherwise, f must be equal to $Cx^{-\alpha}$ for some $C \neq 0$ and

$$\zeta = \int_I y^{-2\alpha} \mathrm{d}y = (1 - 2\alpha)^{-1}.$$

□

The combination of Theorem 3.1 and Lemma 3.2 yields

Theorem 3.3 *The incoherent state $\rho = (2\pi)^{-1} g(\omega)$ is linearly stable for $K \leq K_c$, where*

$$K_c = \frac{2(1 - 2\alpha)}{\pi g(0)}, \quad \alpha \in (0, 1/2). \tag{3.2}$$

In particular, for Gaussian density $g(\eta) = \mathrm{e}^{-\eta^2/2}/\sqrt{2\pi}$, we have

$$K_c(\alpha) = 2\sqrt{\frac{2}{\pi}}(1 - 2\alpha).$$

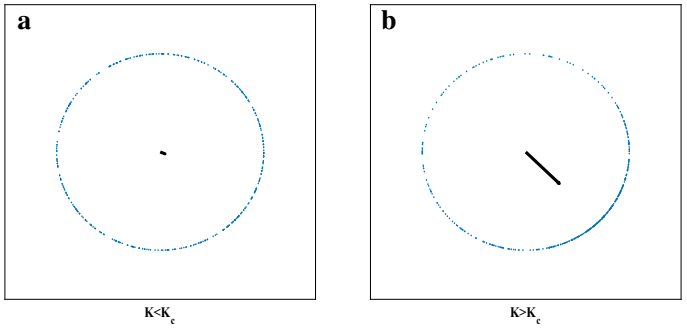

Fig. 2 The distribution of the phases of coupled oscillators is shown on the unit circle in the complex plane: $v_{nk} \mapsto e^{iv_{nk}} \in \mathbb{C},\ k \in [n]$. The strength of coupling is below the critical value K_c in **a** and is above K_c in **b**. The black arrow depicts the order parameter, as a vector in the complex plane (cf. (4.7)). The bigger size (modulus) of the order parameter corresponds to the higher degree of coherence. In **a**, the modulus of the order parameter is close to zero, and the distribution of the oscillators is close to the uniform distribution. In contrast in **b**, the distribution develops a region of higher density. The order parameter points to the expected value (center of mass) of the distribution of the oscillators around $\mathbb{S}$

For $K \leq K_c$, the incoherent state is linearly stable and the oscillators are distributed approximately uniformly around $\mathbb{S}$ (see Fig. 2a). For values of $K > K_c$, numerics show a smooth transition to synchronization (see Figure 9 in Chiba et al. 2018). Note that the synchronization threshold (3.2) can be made arbitrarily small by taking α close to $1/2$. Such good synchronizability of the network is an implication of the scale-free connectivity.

4 Repulsive Coupling

4.1 The Model and Motivating Examples

In the previous section, we found that the incoherent state is linearly stable for $K \leq K_c = \frac{2(1-2\alpha)}{\pi g(0)}$ and is unstable otherwise. For increasing values of $K > K_c$, the asymptotic state of the systems becomes more and more coherent and approaches complete synchronization as $K \to \infty$. In this section, we focus on pattern formation in repulsively coupled networks, i.e., we consider (2.6) with $K < 0$. In this case, the incoherent state is stable, but as we will see below, there are many other stable states. To make the model analytically tractable, we set the intrinsic frequencies equal to the same value $\eta_i = \eta,\ i \in [n]$. By switching to a uniformly rotating frame of coordinates, without loss of generality we assume $\eta = 0$.

Thus, in the remainder of this section, we will be dealing with the following model

$$\dot{u}_{ni} = (n\rho_n)^{-1} \sum_{j=1}^{n} \xi_{nij}(\omega) \sin(u_{ni} - u_{nj}), \quad i \in [n], \tag{4.1}$$

$$u_{ni}(0) = u_{ni}^0. \tag{4.2}$$

Here, we set K to -1, since this can always be achieved by rescaling time.

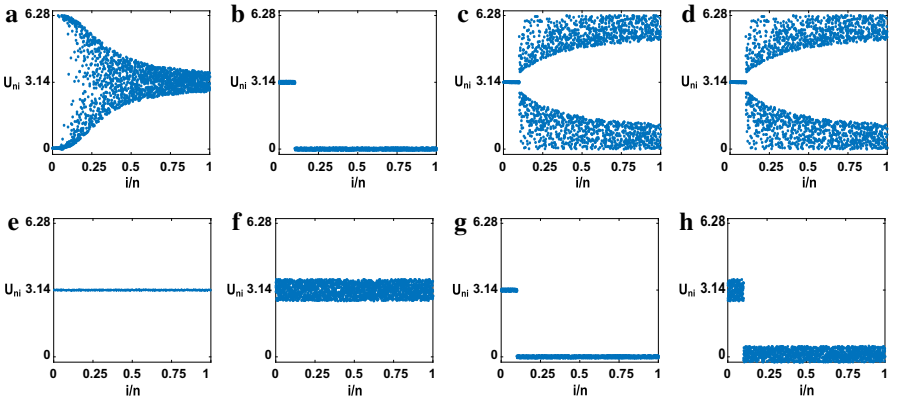

Fig. 3 Plots **a**–**d** show the asymptotic states of model (4.1) initialized by random initial data shown in plots **e**–**h**

After averaging and approximating $\bar{W}_{nij}$ by W_{nij} [cf. (2.10)], we arrive at a counterpart of (2.9)

$$\dot{v}_{ni} = n^{-1} \sum_{j=1}^{n} W_{nij} \sin(v_{ni} - v_{nj}), \quad i \in [n]. \tag{4.3}$$

The corresponding mean field equation is given by

$$\frac{\partial}{\partial t}\rho(t,u,x) + \frac{\partial}{\partial u}\{V(t,u,x)\rho(t,u,x)\} = 0, \tag{4.4}$$

where

$$V(t,u,x) = \int_{\mathbb{S}}\int_{I} W(x,y)\sin(u-v)\rho(t,v,y)\mathrm{d}v\mathrm{d}y. \tag{4.5}$$

In the KM with repulsive coupling on any undirected graph, the synchronous state is unstable (cf. Medvedev and Tang 2015, Theorem 3.7). Thus, it is unstable for the KM on power law graphs (4.1). Instead, we find a variety of stable steady-state solutions. This is the main focus of this section.

We begin with an overview of the representative spatial patterns. First, we initialize (4.1) with conditions sampled uniformly from the n-cube $[\pi-\delta, \pi+\delta]^n$ with sufficiently small $\delta > 0$. Plots a, b of Fig. 3 show asymptotic states corresponding to the initial data shown in Fig. 3e, f, respectively. Note how changing the initial distribution in f affects the corresponding asymptotic state in b.

For our next set of experiments, we choose initial condition from the uniform distribution centered around an antiphase state

$$\bar{u}_n^{(m)} = (\underbrace{0,0,\ldots,0}_{m},\underbrace{\pi,\pi,\ldots,\pi}_{n-m}), \quad m \in [n] \tag{4.6}$$

(see Fig. 3g, h), i.e., the uniform distribution on $\prod_{i=1}^{n}[\bar{u}_{ni}^{(m)} - \delta, \bar{u}_{ni}^{(m)} + \delta]$ for some $m \in [n]$. Note that like in the first pair of examples, the asymptotic states in Fig. 3c,

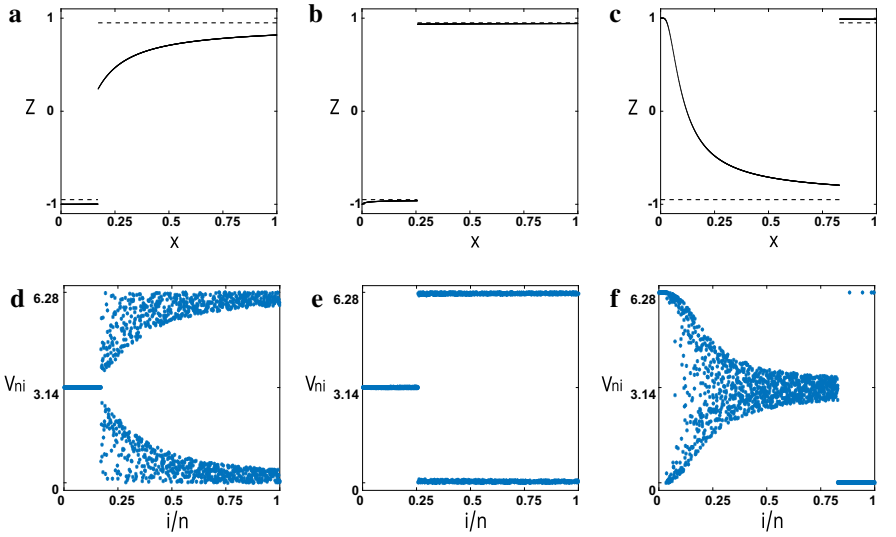

Fig. 4 The initial conditions (dashed line) and asymptotic states (solid line) for (4.22) (**a**–**c**) and the corresponding steady states of (4.3) (**d**–**f**). The patterns shown in **d** and **f** are the examples of contrast states. In **d**, the oscillators in the left region (I^-) are localized around π and are spread-out around 0 in the right region I^+. Similarly, the pattern shown in **f** features localized distribution around 0 and the spread-out one around π

d reflect the changes in the initial conditions. Furthermore, the step-like form of the initial condition translates into the shape of asymptotic states: the oscillators $u_{ni}(t)$ for $i \in [m]$ and those for $i \in [n]/[m]$ exhibit qualitatively different distributions. The oscillators in the former group are tightly localized around π, whereas the oscillators in the latter group show significant variability (see Fig. 3c, d). The oscillators in both groups exhibit well-defined distributions. We call stable (random) spatial patterns, like those in Fig. 3c, d, exhibiting two or more types of qualitatively distinct probability distributions, *contrast states*. By changing $m \in [n]$ in the distribution of the initial condition $\prod_{i=1}^{n}[\bar{u}_{ni}^{(m)}-\delta, \bar{u}_{ni}^{(m)}+\delta]$, we can control the position of the interface between the regions with distinct behaviors (see Fig. 4d–f).

Since the initial data shown in Fig. 3e–h are sampled from an absolutely continuous distribution, the solution of the IVP (4.1), (4.2) for every $t > 0$ is a continuous random vector (cf. Neunzert 1978; Kaliuzhnyi-Verbovetskyi and Medvedev 2018). The density function describing the distributions of $u_{ni}(t)$, $i \in [n]$, is approximated by the solution of the IVP (2.11), (2.13) (cf. Kaliuzhnyi-Verbovetskyi and Medvedev 2018). The analysis of the mean field equation (2.11) explains the transformations of the asymptotic states shown in Figs. 3 and 4.

4.2 The Lyapunov Function

Before turning to the analysis of the mean field equation, we establish several general properties of the ω-limit set of (4.1).[4]

[4] See Guckenheimer and Holmes (1990) for the definition of the ω–limit set.

For the classical KM on complete graphs, Kuramoto introduced the order parameter

$$R_{\rm cmp}(u_n) = n^{-1}\sum_{j=1}^{n} \mathrm{e}^{iu_{nj}}, \quad u_n = (u_{n1}, u_{n2}, \ldots, u_{nn}) \in \mathbb{S}^n. \tag{4.7}$$

to study the transition to synchronization (Kuramoto 1975). The complex-valued order parameter (4.7) provides a convenient measure of coherence in the system dynamics. Indeed, if the phases u_{ni}, $i \in [n]$, are distributed around $\mathbb{S}$ uniformly then $|R_{\rm cmp}(u_n)| \approx 0$, whereas if they evolve in synchrony then $|R_{\rm cmp}(u_n)| \approx 1$.

For the KM on weighted graphs (4.3), there is a suitable generalization of the order parameter:[5]

$$R(u_n) = n^{-1}\sum_{j=1}^{n} a_{nj}\mathrm{e}^{iu_{ni}}, \quad a_{ni} = x_{ni}^{-\alpha}, \ i \in [n]. \tag{4.8}$$

Using $R(u_n)$, (4.3) can be rewritten as follows

$$\dot{u}_{ni} = a_{ni}|R(u_n)|\sin(u_{ni} - \psi), \ i \in [n], \tag{4.9}$$

where $\psi = \mathrm{Arg}\, R(u_n)$. As follows from (4.9), there are two classes of equilibria of (2.9):

$$\begin{aligned}
\mathcal{E}_{n,1} &= \left\{u_n \in \mathbb{S}^n : \ (R(u) \neq 0) \ \& \ \left(u_{nj} - u_{ni} \in \{0, \pi\}, \ \forall i, j \in [n]\right)\right\}, \\
\mathcal{E}_{n,2} &= \left\{u_n \in \mathbb{S}^n : \ R(u_n) = 0\right\}.
\end{aligned}$$

Theorem 4.1 *The ω-limit set of* (4.3) *is* $\mathcal{E}_{n,1} \cup \mathcal{E}_{n,2}$.

Proof Let

$$L(u_n) = \frac{1}{2n}|R(u_n)|^2 \tag{4.10}$$

and note that

$$\begin{aligned}
2nL(u_n) &= \left[n^{-1}\sum_{j=1}^{n} a_{nj}\cos u_{ni}\right]^2 + \left[n^{-1}\sum_{j=1}^{n} a_{nj}\sin u_{ni}\right]^2 \\
&= n^{-2}\sum_{i,j=1}^{n} a_{ni}a_{nj}\cos(u_{ni} - u_{nj})
\end{aligned} \tag{4.11}$$

Further,

$$\frac{\partial}{\partial u_{ni}}L(u_n) = -n^{-1}\sum_{j=1}^{n} a_{ni}a_{nj}\sin(u_{ni} - u_{nj}). \tag{4.12}$$

[5] This order parameter is used in the analysis of the bifurcation underlying the transition to synchrony in the Kuramoto model on graphs (Chiba and Medvedev 2016, 2017). A similar order parameter was used by Laing for the analysis of chimera states in a ring of coupled oscillators (Laing 2009).

Thus, (4.9) is a gradient system

$$\dot{u}_n = -\nabla L(u_n).$$

and

$$\dot{L} = (\nabla L(u_n), \dot{u}_n) = -(\dot{u}_n, \dot{u}_n) \leq 0, \tag{4.13}$$

where $(\cdot, \cdot)$ stands for the inner product in $\mathbb{R}^n$. By the Barbashin–Krasovskii–Lasalle extension of the Lyapunov's direct method (Barbašin and Krasovskiĭ 1952; Krasovskiĭ 1959; LaSalle 1960), we conclude that the ω-limit set of (2.9) is the set of equilibria $\mathcal{E}_{n,1} \cup \mathcal{E}_{n,2}$. □

4.3 Stability of Equilibria in $\mathcal{E}_{n,1}$

In this subsection, to gain first insights into the asymptotic states of the repulsively coupled KM, we study stability of phase locked steady states of (4.9).

By the definition of $\mathcal{E}_{n,1}$, for $u_n = (u_{n1}, u_{n2}, \ldots, u_{nn}) \in \mathcal{E}_{n,1}$ we have $u_{nj} - u_{ni} \in \{0, \pi\}$, $\forall\, i, j \in [n]$. Thus, up to translation by a constant vector

$$\mathcal{E}_{n,1} = \bigcup_{m=1}^{n} \mathcal{E}_{n,1}^{(m)},$$

where $\mathcal{E}_{n,1}^{(m)}$ consists of equilibria with precisely m coordinates equal to 0 and the rest to π. For example,

$$(\underbrace{0, 0, \ldots, 0}_{m}, \underbrace{\pi, \pi, \ldots, \pi}_{n-m}) \in \mathcal{E}_{n,1}^{(m)}. \tag{4.14}$$

Suppose $u_n^{(m)} = (u_{n1}^{(m)}, u_{n2}^{(m)}, \ldots, u_{nn}^{(m)}) \in \mathcal{E}_{n,1}^{(m)}$ for some $m \in [n]$. Then, there is an m-element subset $\Lambda_n^{(m)} \subset [n]$, $|\Lambda_n^{(m)}| = m$ such that

$$u_{n,i}^{(m)} = \begin{cases} 0, & i \in \Lambda_n^{(m)}, \\ \pi, & i \notin \Lambda_n^{(m)}. \end{cases} \tag{4.15}$$

Denote the matrix of linearization of (4.1) about $u_n^{(m)}$ by A. A straightforward computation shows that

$$A = D - vv^{\mathsf{T}}, \tag{4.16}$$

where $D = (d_{ij})$ is a diagonal matrix with nonzero entries

$$d_{ii} = \begin{cases} x_{ni}^{-\alpha} d, & i \in \Lambda_n^{(m)}, \\ -x_{ni}^{-\alpha} d, & i \notin \Lambda_n^{(m)}, \end{cases} \quad d := n^{-1} \sum_{j=1}^{n} (-1)^{\sigma(j)} x_{nj}^{-\alpha}, \tag{4.17}$$

$$v = \left((-1)^{\sigma(1)} x_{n1}^{-\alpha}, (-1)^{\sigma(2)} x_{n2}^{-\alpha}, \ldots, (-1)^{\sigma(n)} x_{nn}^{-\alpha} \right), \quad \sigma(i) = \begin{cases} 0, & i \in \Lambda_n^{(m)}, \\ 1, & i \notin \Lambda_n^{(m)}. \end{cases} \tag{4.18}$$

Lemma 4.2 *For $u \in \mathcal{E}_{n,1}^{(m)}$, $m \in [n]$, let A denote the matrix of linearization of (4.1) about u.*

If $d > 0$ then A has $m-1$ positive eigenvalues, $n-m$ negative eigenvalues, and one zero eigenvalue.

If $d < 0$ then A has $n-m-1$ positive eigenvalues, m negative eigenvalues, and one zero eigenvalue.

Corollary 4.3 *All equilibria from $\mathcal{E}_{n,1}^{(m)}$, $1 < m \leq n$, are unstable. In particular, all solutions of form (4.14) are unstable for $m > 1$.*

Proof of Lemma 4.2 Suppose $d > 0$. Let $\lambda_k(D)$, and $\lambda_k(A)$ $k \in [n]$, denote the eigenvalues of D and A arranged in the increasing order counting multiplicity. Since $A = D - vv^{\mathsf{T}}$, from the Weyl's theorem (Horn and Johnson 2013, Corollary 4.3.3) we immediately have

$$\lambda_{n-m}(A) \leq \lambda_{n-m}(D) < 0.$$

Further, the interlacing theorem (Horn and Johnson 2013, Theorem 4.3.4) implies

$$0 < \lambda_{n-m+1}(D) \leq \lambda_{n-m+2}(A).$$

Finally, there is at least one zero eigenvalue of A, because its rows sum is equal to 0. Thus, A has precisely $n-m$ negative, $n-m+1$ positive eigenvalues, and one zero eigenvalue.

The case $d < 0$ is analyzed similarly. □

4.4 The Ott–Antonsen Ansatz

Unlike equilibria in $\mathcal{E}_{n,1}$ considered in the previous subsection, equilibria in $\mathcal{E}_{n,2}$ are harder to identify explicitly. To study properties of the equilibria in $\mathcal{E}_{n,2}$, we will invoke the mean field equation:

$$\frac{\partial}{\partial t}\rho(t,u,x) + \frac{\partial}{\partial u}\{V(t,u,x)\rho(t,u,x)\} = 0, \tag{4.19}$$

where

$$V(t,u,x) = \int_I \int_{\mathbb{S}} W(x,y)\sin(u-v)\rho(t,v,y)\mathrm{d}v\mathrm{d}y. \tag{4.20}$$

To identify a class of stable steady states of (4.19), we employ the Ott–Antonsen ansatz (Ott and Antonsen 2008), i.e., we look for solutions of (4.19) in the following form:

$$\rho(t,u,x) = \frac{1}{2\pi}\left(1 + \sum_{k=1}^{\infty}\left(\overline{z(t,u)}^k \mathrm{e}^{iku} + z(t,u)^k \mathrm{e}^{-iku}\right)\right). \tag{4.21}$$

If $\sup_{x\in I, t\in[0,T]} |z(t,x)| < 1$ then the series on the right-hand side of (4.21) is absolutely convergent. Plugging (4.21) into (4.19), after straightforward albeit tedious

manipulations, one verifies that (4.21) solves (4.19), provided $z(t,x)$ satisfies the following equation

$$\frac{\partial}{\partial t} z(t,x) = \frac{1}{2x^\alpha}\left(z(t,x)^2 - 1\right)\mathcal{R}[z(t,\cdot)], \tag{4.22}$$

where

$$\mathcal{R}[v] = \int_I y^{-\alpha} v(y)\mathrm{d}y. \tag{4.23}$$

From (4.21), it follows that

$$z(t,x) = \int_0^{2\pi} \rho(t,u,x)\mathrm{e}^{iu}\mathrm{d}u. \tag{4.24}$$

Using (4.24), we can express $\mathcal{R}[z]$ in terms of the density ρ:

$$\mathcal{R}[z] = \int_I \int_{\mathbb{S}} y^{-\alpha}\rho(t,u,y)\mathrm{e}^{iu}\mathrm{d}u\mathrm{d}y, \tag{4.25}$$

i.e., $\mathcal{R}[z]$ is the continuous counterpart of the order parameter (4.8).

Below, we will consider solutions of (4.19) subject to initial conditions that are even functions in u for every $x \in I$. Since the flow respects this symmetry, the solutions of the initial value problem for (4.19) are even functions in u for every t and x. In this case, $z(t,x)$ is real as easily seen from (4.24). In the remainder of this section, we restrict to real solutions of (4.22). It is instructive to review the interpretation of $z(t,x)$ (cf. Omelchenko 2013). To this end, note that (4.21) implies

$$\rho(t,u,x) = \frac{1 - |z(t,x)|^2}{2\pi\left(1 - 2|z(t,x)|\cos(u - \mathrm{Arg}\ z(t,x)) + |z(t,x)|^2\right)}. \tag{4.26}$$

In particular, $z \equiv 0$ corresponds to the uniform density, while values of z close to ± 1 indicate that the density is concentrated around 0 and π, respectively. Note that the Ott–Antonsen ansatz assumes that the initial condition for ρ is consistent with (4.26). Thus, it applies only to a special class of solutions of the mean field equation (4.19), (4.20). Nonetheless, the analysis of the mean field equation using the Ott–Antonsen ansatz gives valuable insights into the dynamics of the couples system and explains the transformations of the asymptotic states shown in Fig. 3.

4.5 The Nonlocal Equation

Let $\mathcal{M}(0,1)$ be a space of measurable functions $z : (0,1] \to [-1,1]$. In analogy to the discrete model (4.1), we divide the equilibria of (4.22) into two classes:

$$\tilde{\mathcal{E}}_1 = \{z \in \mathcal{M}(0,1) :\ (|z(x)| = 1,\ x \in (0,1])\&(\mathcal{R}[z] \neq 0)\},$$
$$\tilde{\mathcal{E}}_2 = \{z \in \mathcal{M}(0,1) :\ \mathcal{R}[z] = 0\}.$$

Theorem 4.4 *Let $z_0 \in \mathcal{M}(0,1)\backslash\tilde{\mathcal{E}}_1$. Denote by $\omega(z_0)$ the ω–limit set of the trajectory of (4.22) started at z_0. Then, $\omega(z_0) \subset \tilde{\mathcal{E}}_2$.*

Proof Suppose $\mathcal{R}(0) := \mathcal{R}[z(0,\cdot)] > 0$. Changing the time variable to $t = \eta(\tau)$ subject to

$$\eta'(\tau) = \frac{1}{\int_I y^{-\alpha}\tilde{z}(\tau, y)dy}, \quad \tilde{z}(\tau, y) := z(\eta(\tau), x), \quad \eta(0) = 0, \tag{4.27}$$

we reduce (4.22) to

$$\frac{\partial}{\partial\tau}\tilde{z} = \frac{1}{2x^\alpha}\left(\tilde{z}^2 - 1\right). \tag{4.28}$$

The last equation is integrated explicitly

$$\tilde{z}(\tau, x) = \frac{1 - C(x)\exp\{\frac{\tau}{x^\alpha}\}}{1 + C(x)\exp\{\frac{\tau}{x^\alpha}\}}, \quad C(x) = \frac{1 - z_0(x)}{1 + z_0(x)}. \tag{4.29}$$

Clearly, $\tilde{z}(\tau, x) \searrow -1$ for $x \in I$ as $\tau \to \infty$. Thus, there is $0 < \tau^* < \infty$ such that $\tilde{\mathcal{R}}(\tau^*) := \tilde{\mathcal{R}}[\tilde{z}(\tau^*, \cdot)] = 0$ and $\tilde{\mathcal{R}}(\tau) > 0$ for $\tau \in [0, \tau^*)$.

The change in time (4.27) is well defined for $\tau \in [0, \tau^*)$. In terms of the original time, we have the description of the system's dynamics on the time interval $[0, t^*)$, with

$$t^* = \lim_{\tau\to\tau^*-0}\int_0^\tau (\tilde{\mathcal{R}}(s))^{-1}\mathrm{d}s. \tag{4.30}$$

Denote $\mathcal{R}(t) = \mathcal{R}[z(t,\cdot)]$. If $t^* < \infty$ then $\mathcal{R}(t) = \tilde{\mathcal{R}}(\tau^*) = 0$ for $t \geq t^*$. Otherwise, multiplying both sides of (4.22) by $x^{-\alpha}$ and integrating over I, we have

$$\begin{aligned}
\mathcal{R}' &= 2^{-1}\int_I x^{-2\alpha}(z^2(x,t) - 1)\mathrm{d}x\,\mathcal{R} \\
&\leq 2^{-1}\int_I x^{-2\alpha}(z(x,t) - 1)\mathrm{d}x\,\mathcal{R} \\
&\leq 2^{-1}\int_I x^{-\alpha}(z(x,t) - 1)\mathrm{d}x\,\mathcal{R} \\
&\leq \left(\mathcal{R} - (1-\alpha)^{-1}\right)\mathcal{R}.
\end{aligned} \tag{4.31}$$

By the comparison principle (cf. Hartman 1973, Theorem I.4.1), from (4.31) we conclude that $\mathcal{R}(t) \searrow 0$, as $t \to \infty$.

The case $\mathcal{R}[z(0,\cdot)] < 0$ is analyzed similarly. □

4.6 Attractors of the Repulsively Coupled Model

Theorem 4.4 shows that solutions of the mean field equation of form (4.21) approach an equilibrium from the set $\{\mathcal{R} = 0\}$. To illustrate possible patterns generated in this scenario, we consider the IVP for (4.22) with the following initial conditions:

$$z^{(step)}_{\delta,x_0}(x) = \begin{cases} -1+\delta, & x \in I^- := (0, x_0), \\ 1-\delta, & x \in I^+ := [x_0, 1), \end{cases} \tag{4.32}$$

Remark 4.5 The initial condition for the mean field equation (4.19) is obtained by plugging (4.32) into (4.26). It is sufficiently close to the uniform density used in the numerical simulations in Fig. 3, albeit is not the same. Still the analysis of the nonlocal equation with the initial condition (4.32) explains the solutions shown in Fig. 3. The uniform distribution in simulations was used for convenience. The results change little if (4.26), (4.32) is used as the initial condition for (4.19).

For $0 < \delta \ll 1$, $z^{(\text{step})}_{\delta,x_0}$ is close to the equilibrium $z^{(\text{step})}_{0,x_0} \in \tilde{\mathcal{E}}_1$, corresponding to a phase locked solution, localized around π for $x \in I^-$ and around 0 for $x \in I^+$.

Consider the IVP for (4.22) with initial condition $z^{(\text{step})}_{\delta,x_0}$ for $0 < \delta < 1$. To this end, note that for $x^* = 2^{\frac{-1}{1-\alpha}} \in (0, 1)$,

$$\int_0^{x^*} y^{-\alpha} \mathrm{d}y = -\int_{x^*}^1 y^{-\alpha} \mathrm{d}y.$$

Suppose first that $0 < x_0 < x^*$. Then $\mathcal{R}(0) > 0$. By Theorem 4.4, $\mathcal{R}(t) \searrow 0$. Furthermore, $|z(t, x)| \le 1$ and, thus, $z(t, x)$ is monotonically decreasing in time for every $x \in (0, 1]$. In particular,

$$-1 \le z(t, x) \le -1 + \delta, \quad x \in I^- = (0, x_0), \ t \ge 0. \tag{4.33}$$

This means that in I^- the oscillators remain localized around π (in the moving frame of coordinates) [cf. (4.26)], provided $0 < \delta \ll 1$ (Fig. 4d). On the other hand, in I^+, $z(t, \cdot)$ is monotonically decreasing to its asymptotic state z_∞ at which $\mathcal{R}(z_\infty) = 0$ (see Fig. 4a). In I^+, there must be an interval over which z is positive and strictly less than $1 - \delta$ for all times. Denote such interval $\tilde{I}^+ \subset I^+$. Thus, over $\tilde{I}^+$, $z(t, x)$ is bounded away from ± 1 by a distance greater than δ uniformly in time. Thus, the oscillators over $\tilde{I}^+$ exhibit a greater degree of incoherence. The asymptotic state z_∞ contains both the region of coherent dynamics (I^-) and that of incoherent (I^+) (Fig. 4a). Thus, z_∞ corresponds to a contrast state. This is clearly seen in numerics (see Fig. 4d). In the next section, for the modified model we will present tight estimates characterizing the asymptotic state z_∞.

Next, we comment on the transformation of the asymptotic state z_∞ as x_0 is increasing past x^*. The case of $x > x^*$ presents a symmetric scenario. In this case, $\mathcal{R}(0) < 0$ and both $\mathcal{R}(t)$ and $z(t, \cdot)$ are monotonically increasing (see Fig. 4c). In particular, $1 - \delta \le z(t, x) \le 1$ in I^+ for $t \ge 0$, and the oscillators are localized around 0 in I^+, while exhibiting incoherent behavior in I^- (see Fig. 4c, f). When x_0 is close to x^*, $\mathcal{R}(0)$ is close to zero, and $|\mathcal{R}(t)|$ remains small for all times. This means that the initial pattern does not change much in the process of evolution, and z_∞ remains close to the step function

$$z^{(\text{step})}_{0,x_0}(x) := \pm 1, \ x \in I^\pm.$$

The equilibrium $z^{(\mathrm{step})}_{0,x_0} \in \tilde{\mathcal{E}}_1$ is unstable but lies close a stable equilibrium $z_{\mathrm{step},x^*} \in \tilde{\mathcal{E}}_2$ (see Fig. 4b, e).

4.7 Contrast States in the Modified KM

We now turn to a modification of the KM on power law graphs, for which we derive tight estimates for the contrast states. If instead of scaling the coupling term by $n\rho_n$, as in (2.6), we scale it by the expected degree of node i:

$$d_{ni} = \mathbb{E}_{\,\omega} \deg_{\Gamma_n}(i) = \sum_{j=1}^{n} \bar{W}_{nij},$$

the repulsively coupled KM and the corresponding averaged equation take the following form:

$$\dot{u}_{ni} = \frac{1}{d_{ni}} \sum_{j=1}^{n} \xi_{nij}(\omega) \sin(u_{ni} - u_{nj}), \quad i \in [n], \tag{4.34}$$

and

$$\dot{v}_{ni} = \frac{1}{n} \sum_{j=1}^{n} x_{nj}^{-\alpha} \sin(v_{ni} - v_{nj}), \quad i \in [n], \tag{4.35}$$

respectively. The mean field equation then becomes (cf. Kaliuzhnyi-Verbovetskyi and Medvedev 2017, Example 2.5)

$$\frac{\partial}{\partial t}\rho(t,u,x) + \frac{\partial}{\partial u}\left\{\rho(t,u,x)\int_I\int_S (1-\alpha)y^{-\alpha}\sin(u-v)\rho(t,v,y)\mathrm{d}v\mathrm{d}y\right\}. \tag{4.36}$$

Applying the Ott–Antonsen ansatz to the model at hand, we arrive at

$$\dot{z} = \frac{1-\alpha}{2}\left(z^2-1\right)\mathcal{R}[z]. \tag{4.37}$$

For (4.37) subject to the initial condition (4.32), below we present tight bounds for the large time asymptotic state z_∞.

Suppose $\mathcal{R}[z(0,\cdot)] > 0$ and note that (4.37) and (4.32) imply

$$|z(x,t)| \le 1 \quad \text{and} \quad \mathcal{R}[z(t,\cdot)] \ge 0,$$

for any $x \in I$ and $t \ge 0$. Furthermore, $z(t,x)$ is monotonically decreasing.

On the other hand, from (4.37) we have

$$(1-\alpha)(z-1)\mathcal{R}[z(t,\cdot)] \le \frac{\partial}{\partial t}z \le \frac{1-\alpha}{2}(z-1)\mathcal{R}[z(t,\cdot)]. \tag{4.38}$$

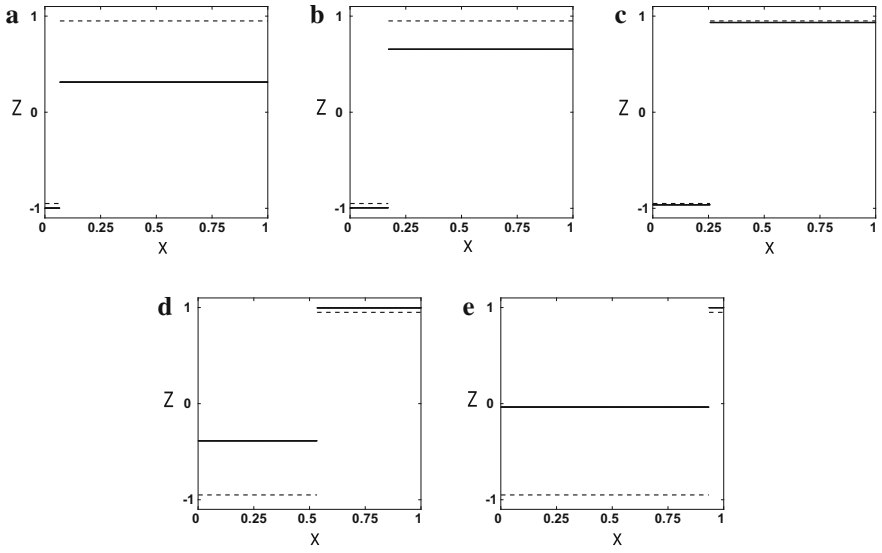

Fig. 5 The initial conditions (dashed line) and asymptotic states (solid line) for (4.37)

Multiplying all sides of the double inequality (4.38) by $x^{-\alpha}$ and integrating over I, we have

$$((1-\alpha)\mathcal{R}[z(t,\cdot)]-1) \le \frac{\partial}{\partial t}\mathcal{R}[z(t,\cdot)] \le 2^{-1}\left((1-\alpha)\mathcal{R}[z(t,\cdot)]-1\right). \tag{4.39}$$

Recalling $\mathcal{R}[z(0,\cdot)] > 0$, $\mathcal{R}[z(t,\cdot)] \searrow 0$ as $t \to \infty$, i.e., $z(t,\cdot)$ approaches an equilibrium from $\tilde{\mathcal{E}}_2$. Next, we characterize the limiting state of the system. Since the initial condition is constant over each of the intervals $I^{\pm}$, so is the solution (Fig. 5)

$$\begin{aligned} z(x,t) &\equiv z^-(t), \quad x \in I^-, \\ z(x,t) &\equiv z^+(t), \quad x \in I^+, \end{aligned} \tag{4.40}$$

Since $z^-(0) = -1+\delta$ and $z^-(t) \ge -1$, we have

$$\left|z^-(t)+1\right| \le \delta, \tag{4.41}$$

i.e., the solution of the repulsively coupled KM (4.1) remains approximately synchronized over I^-.

Denote

$$z_\infty^{\pm} := \lim_{t\to\infty} z^{\pm}(t).$$

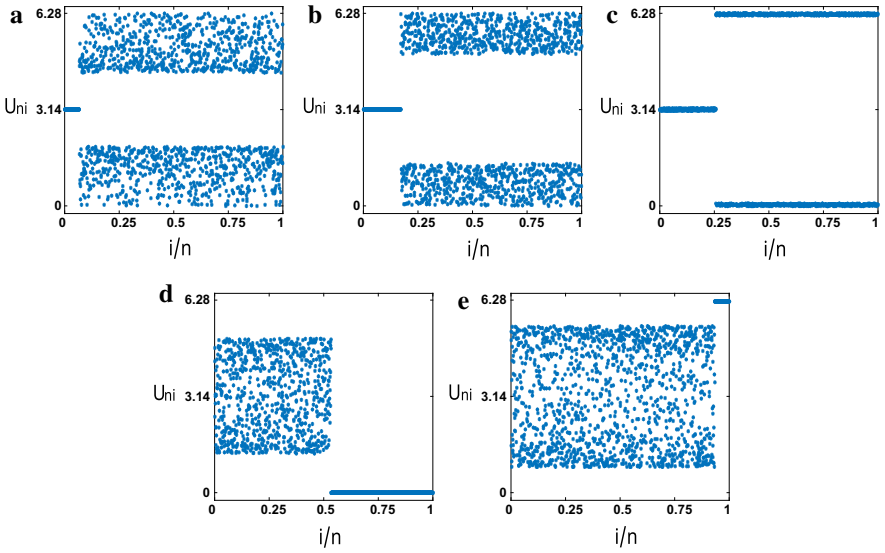

Fig. 6 The asymptotic states of (4.34). The patterns in **a**–**d** correspond to the solutions of (4.37) shown in the corresponding plots of Fig. 5

Further, since $\Re[z(t,\cdot)] \to 0$ as $t \to \infty$, we have

$$z_\infty^+ \int_{x_0}^1 y^{-\alpha} \mathrm{d}y = -z_\infty^- \int_0^{x_0} y^{-\alpha} \mathrm{d}y.$$

and

$$z_\infty^+ = -z_\infty^- \frac{x_0^{1-\alpha}}{1 - x_0^{1-\alpha}}. \tag{4.42}$$

The combination of (4.41) and (4.42) yields

$$(1-\delta)\frac{x_0^{1-\alpha}}{1 - x_0^{1-\alpha}} \le z_\infty^+ \le \frac{x_0^{1-\alpha}}{1 - x_0^{1-\alpha}}. \tag{4.43}$$

This double inequality combined with (4.41) yields tight estimates for the asymptotic state z_∞ in I^+. Estimates (4.41) and (4.43) characterize the asymptotic states for initial conditions $\Re[z(0,\cdot)] > 0$ (Fig. 5a, b). The complementary case $\Re[z(0,\cdot)] > 0$ is analyzed similarly. The corresponding contrast states are shown in Fig. 6.

5 Discussion

Networks with power law degree distribution feature prominently in applications (Barabási and Albert 1999). These are complex networks, whose structure is

defined implicitly through the statistics of degrees of the vertices. Understanding dynamics of coupled systems on such networks is a challenging problem. In this paper, we employed the framework of sparse W-random graphs (Borgs et al. 2014) to develop an analytically tractable coupled oscillator model on power law graphs. In this paper, we focus on the KM of coupled phase oscillators; however, our approach extends naturally to other types of coupled dynamical systems on graphs. For the KM on graphs, we derived the mean field partial differential equation approximating the dynamics of the coupled system in the limit as the size of the network tends to infinity. A precise mathematical interpretation of the mean field for the KM on graphs has been recently provided in Chiba and Medvedev (2016), Kaliuzhnyi-Verbovetskyi and Medvedev (2018).

The mean field equation was used to calculate the synchronization threshold for the model with attractive coupling and to study pattern formation in the repulsively coupled model. The analysis of the synchronization problem revealed a remarkable feature of the power law connectivity: the synchronization threshold can be made arbitrarily close to zero by controlling the parameter of the power law distribution. For repulsively coupled model with identical intrinsic frequencies, we performed a detailed analysis of stable steady states. A striking feature of the repulsively coupled model is the existence of a family of equilibria, which form a co-dimension 2 manifold. Given an initial condition, the large time asymptotic state of the system is selected from this rich set of equilibria. Furthermore, the asymptotic state is controlled by the initial condition in practically continuous manner, i.e., small changes in the initial data result in small changes in the asymptotic state. This property is not be confused with continuous dependence on initial data on finite time intervals.

We analyzed the relation between the initial data and the asymptotic state for a special class of initial conditions fitting into the Ott–Antonsen ansatz (Ott and Antonsen 2008). The use of the ansatz allows to see explicitly how the initial condition translates into the asymptotic state of the system. It also reveals the mechanism for the creation of contrast states, steady-state solutions, which like chimera states (Omelchenko 2013), have multiple sets of oscillators subject to qualitatively distinct probability distributions. The contrast states identified in this work and chimera states have the same nature, as can be seen by comparing our analysis to the analysis of chimera states in Omelchenko (2013). At the heart of the existence of multiple regions with distinct behaviors in both cases lies the piecewise structure of the attractors of the nonlocal equation derived via the Ott–Antonsen ansatz [compare Fig. 4a–c with the plots for $|a(x)|$ in Figure 3 of Omelchenko (2013)]. In our case, the situation is simpler, because it involves steady states compared to the periodic orbits in Omelchenko (2013). Taken together, the results of this paper suggest an analytic approach to modeling and analysis of coupled dynamical systems on power law graphs and illustrate implications of the power law connectivity for the dynamics of coupled systems.

Acknowledgements This work was supported in part by the NSF DMS grants 1412066 and 1715161 (to GM).

References

Abrams, D.M., Strogatz, S.H.: Chimera states in a ring of nonlocally coupled oscillators. Int. J. Bifurc. Chaos Appl. Sci. Eng. **16**(1), 21–37 (2006)

Barabási, A.-L., Albert, R.: Emergence of scaling in random networks. Science **286**(5439), 509–512 (1999)

Barbašin, E.A., Krasovskiĭ, N.N.: On stability of motion in the large. Doklady Akad. Nauk SSSR (N.S.) **86**, 453–456 (1952)

Borgs, C., Chayes, J., Lovász, L., Sós, V., Vesztergombi, K.: Limits of randomly grown graph sequences. Eur. J. Combin. **32**(7), 985–999 (2011)

Borgs, C., Chayes, J.T., Cohn, H., Zhao, Y.: An L^p theory of sparse graph convergence I: limits, sparse random graph models, and power law distributions. (2014). arXiv:1401.2906

Chiba, H.: A proof of the Kuramoto conjecture for a bifurcation structure of the infinite-dimensional Kuramoto model. Ergod. Theory Dyn. Syst. **35**(3), 762–834 (2015)

Chiba, H., Medvedev, G.S.: The mean field analysis for the Kuramoto model on graphs I. The mean field equation and transition point formulas. (2016). arXiv:1612.06493

Chiba, H., Medvedev, G.S.: The mean field analysis of the Kuramoto model on graphs II. Asymptotic stability of the incoherent state, center manifold reduction, and bifurcations. (2017). arXiv:1709.08305

Chiba, H., Nishikawa, I.: Center manifold reduction for large populations of globally coupled phase oscillators. Chaos **21**(4), 043103–043110 (2011)

Chiba, H., Medvedev, G.S., Mizuhara, M.S.: Bifurcations in the Kuramoto model on graphs. Chaos. **28**, 073109 (2018). (**in press**)

Chung, F., Lu, L.: The average distances in random graphs with given expected degrees. Proc. Natl. Acad. Sci. USA **99**(25), 15879–15882 (2002)

Dudley, R.M.: Real Analysis and Probability. Cambridge Studies in Advanced Mathematics, vol. 74. Cambridge University Press, Cambridge (2002). Revised reprint of the 1989 original

Golse, F.: On the dynamics of large particle systems in the mean field limit. In: Muntean, A., Rademacher, J., Zagaris, A. (eds.) Macroscopic and Large Scale Phenomena: Coarse Graining, Mean Field Limits and Ergodicity. Lect. Notes Appl. Math. Mech., vol. 3, pp. 1–144. Springer, Cham (2016)

Guckenheimer, J., Holmes, P.: Nonlinear Oscillations, Dynamical Systems, and Bifurcations of Vector Fields. Applied Mathematical Sciences, vol. 42. Springer, New York (1990). Revised and corrected reprint of the 1983 original

Hartman, P.: Ordinary Differential Equations. S. M. Hartman, Baltimore (1973). (**Corrected reprint**)

Hoppensteadt, F.C., Izhikevich, E.M.: Weakly Connected Neural Networks. Applied Mathematical Sciences, vol. 126. Springer, New York (1997)

Horn, R.A., Johnson, C.R.: Matrix Analysis, 2nd edn. Cambridge University Press, Cambridge (2013)

Kaliuzhnyi-Verbovetskyi, D., Medvedev, G.S.: The semilinear heat equation on sparse random graphs. SIAM J. Math. Anal. **49**(2), 1333–1355 (2017)

Kaliuzhnyi-Verbovetskyi, D., Medvedev, G.S.: The mean field equation for the Kuramoto model on graph sequences with non-Lipschitz limit. SIAM J. Math. Anal. **50**(3), 2441–2465 (2018)

Krasovskiĭ, N.N.: Nekotorye zadachi teorii ustoichivosti dvizheniya. Gosudarstv. Izdat. Fiz.-Mat. Lit, Moscow (1959)

Kuramoto, Y.: Self-entrainment of a population of coupled non-linear oscillators. In: International Symposium on Mathematical Problems in Theoretical Physics (Kyoto Univ., Kyoto, 1975). Lecture Notes in Phys., vol. 39, pp. 420–422. Springer, Berlin (1975)

Kuramoto, Y., Battogtokh, D.: Coexistence of coherence and incoherence in nonlocally coupled phase oscillators. Nonlinear Phenom. Complex Syst. **5**, 380–385 (2002)

Laing, C.R.: Chimera states in heterogeneous networks. Chaos **19**(1), 013113–013118 (2009)

Lancellotti, C.: On the Vlasov limit for systems of nonlinearly coupled oscillators without noise. Transp. Theory Stat. Phys. **34**(7), 523–535 (2005)

LaSalle, J.: Some extensions of Liapunov's second method. IRE Trans. Circuit Theory **7**(4), 520–527 (1960)

Lovász, L., Szegedy, B.: Limits of dense graph sequences. J. Comb. Theory Ser. B **96**(6), 933–957 (2006)

Medvedev, G.S.: Stochastic stability of continuous time consensus protocols. SIAM J. Control Optim. **50**(4), 1859–1885 (2012)

Medvedev, G.S.: The nonlinear heat equation on W-random graphs. Arch. Ration. Mech. Anal. **212**(3), 781–803 (2014a)

Medvedev, G.S.: Small-world networks of Kuramoto oscillators. Phys. D **266**, 13–22 (2014b)

Medvedev, G.S.: The continuum limit for the Kuramoto model on sparse random graphs. (2018). arXiv:1802.03787
Medvedev, G.S., Tang, X.: Stability of twisted states in the Kuramoto model on Cayley and random graphs. J. Nonlinear Sci. **25**(6), 1169–1208 (2015)
Medvedev, G.S., Douglas Wright, J.: Stability of twisted states in the continuum Kuramoto model. SIAM J. Appl. Dyn. Syst. **16**(1), 188–203 (2017)
Motsch, S., Tadmor, E.: Heterophilious dynamics enhances consensus. SIAM Rev. **56**(4), 577–621 (2014)
Neunzert, H.: Mathematical investigations on particle-in-cell methods Fluid Dyn. Trans. **9**, 229–254 (1978)
Omelchenko, O.E.: Coherence-incoherence patterns in a ring of non-locally coupled phase oscillators. Nonlinearity **26**(9), 2469 (2013)
Ott, E., Antonsen, T.M.: Low dimensional behavior of large systems of globally coupled oscillators. Chaos **18**, 037113 (2008)
Porter, M.A., Gleeson, J.P.: Dynamical Systems on Networks. Frontiers in Applied Dynamical Systems: Reviews and Tutorials, vol. 4. Springer, Cham (2016). A tutorial
Strogatz, S.H.: From Kuramoto to Crawford: exploring the onset of synchronization in populations of coupled oscillators. Phys. D **143**(1–4), 1–20 (2000)
Strogatz, S.H., Mirollo, R.E.: Stability of incoherence in a population of coupled oscillators. J. Stat. Phys. **63**(3–4), 613–635 (1991)
Wiley, D.A., Strogatz, S.H., Girvan, M.: The size of the sync basin. Chaos **16**(1), 015103–015108 (2006)

Affiliations

Georgi S. Medvedev[1] · Xuezhi Tang[2]

Xuezhi Tang
xuezhi.tang@wellsfargo.com

1 Department of Mathematics, Drexel University, 3141 Chestnut Street, Philadelphia, PA 19104, USA

2 Wells Fargo Securities, 505 S. Tryon Street, Charlotte, NC 28202, USA